Theoretical and Mathematical Physics, **162**(1): 106–125 (2010)

PROPERTIES OF THE HEAVY-FERMION SPECTRUM IN THE CANTED PHASE OF ANTIFERROMAGNETIC INTERMETALLIDES

© **V. V. Val'kov*** **and D. M. Dzebisashvili†**

We study the effect of the magnetic-field-induced canting of magnetic sublattices on the energy structure of heavy fermion quasiparticles in intermetallides with antiferromagnetic-type ordering. We work in the framework of an effective Hamiltonian of the periodic Anderson model in the regime of strong electron correlations. With the virtual transfers into high-energy double states taken into account, this Hamiltonian involves exchange interactions between spin moments of the f ions and the s–f-exchange coupling between the two subsystems. For a noncollinear problem geometry, we introduce a unitary transformation that allows reducing an eighth-order equation for the spectrum of heavy fermions to two fourth-order equations. We show that the quasimomentum dependence of the heavy-fermion energy changes qualitatively under the transition from the antiferromagnetic phase to a phase with a considerable canting angle emerging in an external magnetic field.

Keywords: periodic Anderson model, heavy fermion, antiferromagnetism, canted phase

1. Introduction

The problem of taking the strong electron correlations correctly into account when describing the physical properties of systems based on rare-earth and transuranium elements is central in the modern theory of the condensed state of matter. A characteristic feature of such systems is the existence of an unfilled f shell of rare-earth ions and strong intra-ion Coulomb interactions. The large magnitude of hybridization of the atomic orbitals of magnetic ions with collectivized electron states does not allow considering the conducting and magnetic properties of such systems separately and requires a unified approach for describing them. Theoretical investigations of such systems are based on the periodic Anderson model (PAM) [1].

In compounds with heavy fermions (HFs), Kondo systems, and mixed-valence compounds, the current carrier mobility varies in a wide range. These systems therefore include insulators, semiconductors, metals, and superconductors. Experimental data provide evidence of an essential effect of strong electron correlations (SEC) on the thermodynamic [2]–[5] and galvanomagnetic [6]–[9] properties. To describe the low-temperature behavior of these systems, the slave-boson representation method was proposed [10], which allows taking SEC into account and obtaining the spectrum of HFs with a large effective mass in the case of paramagnetic intermetallides.

Currently, a large class of HF systems and Kondo systems is comprised of materials that pass into a state with long-range antiferromagnetic (AFM) order at lowered temperatures. This ordering in the localized subsystem affects the HF spectrum because current carriers are strongly related to localized moments. In the special case of the PAM with the chemical potential strictly at the midpoint between the energy values E_0 and $E_0 + U$, the Fermi spectrum for a Kondo AFM insulator was calculated in [11]–[14]. But the

*Institute of Physics, Siberian Branch, RAS, Krasnoyarsk, Russia, e-mail: vvv@iph.krasn.ru.

†Federal Siberian University, Krasnoyarsk, Russia, e-mail: ddm@iph.krasn.ru.

Translated from Teoreticheskaya i Matematicheskaya Fizika, Vol. 161, No. 3, pp. 125–149, January, 2010. Original article submitted April 29, 2009.

obtained solutions cannot be used to describe the metallic behavior of AFM intermetallides. Furthermore, these solutions are applicable only for the collinear geometry, with no canting of magnetic sublattices. In isotropic AFM systems, this is possible only in a zero magnetic field ($H = 0$).

On the other hand, a substantial number of experimental works are devoted to studying the properties of AFM HF systems in an external magnetic field. Because the characteristic spin-ordering temperatures of AFM HF systems are a few degrees Kelvin, it follows that magnetic fields $\sim 30\,\text{k}\text{Ø}$ are comparable to the exchange interaction energies. Therefore, such fields can essentially affect the mutual orientation of the magnetic sublattices in the localized subsystem. It is therefore relevant to calculate the HF spectrum in AFM intermetallides in the case where the magnetic field leads to a noticeable canting of the magnetic sublattices. The rearrangement of the ground-state structure of the magnetic subsystem due to the strong coupling with collectivized electrons has an essential impact on their energy spectrum.

In what follows, we use the so-called extended PAM to describe the magnetic properties of HF metal systems; this model takes the exchange interactions in the subsystem of localized f electrons and the s–f-exchange interactions of localized and collectivized electrons into account. Terms of these types occur in the effective low-energy PAM Hamiltonian in the regime of a strong but finite on-site Coulomb interaction U due to the Schrieffer–Wolff transformation [15], [16]. This approach, based on the method of canonical transformations, was used in different versions to construct the effective PAM Hamiltonian in [17]–[21]. But we must note that in the case of AFM HF systems with a metallic-type ground state, the effective exchange integrals resulting from the Schrieffer–Wolff transformation diverge if the energy E_0 of the localized level is inside the conductance band [21]. This obstructions was removed in [22] by segregating high-energy hybridization processes V_{12} that lead to virtual transfers into the upper Hubbard band. With these processes taken into account through the fourth order in the parameter V_{12}/U, an effective PAM Hamiltonian was constructed that describes the above exchange interactions in the metallic phase. This Hamiltonian is used in what follows to calculate the HF spectrum in the canted phase of metallic AFM systems.

2. Effective Hamiltonian of AFM intermetallides

The PAM Hamiltonian in the representation of creation and annihilation operators $c^+_{k\sigma}$ (d^+_f) and $c_{k\sigma}$ (d_f) of a collectivized (localized) electron with the quasimomentum k (with the Wannier cell number f) and spin moment projection σ is given by

$$\widehat{\mathscr{H}} = \sum_{k\sigma}(\varepsilon_{k\sigma} - \mu)c^+_{k\sigma}c_{k\sigma} + \sum_{f\sigma}(E_\sigma - \mu)d^+_{f\sigma}d_{f\sigma} + \\ + U\sum_f \hat{n}_{f\uparrow}\hat{n}_{f\downarrow} + \frac{1}{\sqrt{N}}\sum_{fk\sigma}\{V_k e^{-ikf}c^+_{k\sigma}d_{f\sigma} + \text{c.c.}\}. \quad (1)$$

Here, the first sum describes an ensemble of noninteracting conductance electrons placed in an external magnetic field H lifting the degeneracy of the bare energy spectrum ε_k with respect to the value of the spin moment projection $\sigma = +1/2, -1/2$, $\varepsilon_{k\sigma} = \varepsilon_k - 2\sigma\mu_\text{B}H$, and μ_B is the Bohr magneton. The second term in Hamiltonian (1) accounts for the existence of localized f-electron states with the initial energy E_0 in the intermetallides under consideration. The energy of these states in a magnetic field contains a Zeeman piece $E_\sigma = E_0 - g\sigma\mu_\text{B}H$ depending on the g factor. The chemical potential μ appears in these operator expressions because of the subsequent averaging over the grand canonical ensemble. The Coulomb interaction operator for two electrons in the states localized at a cell f and having opposite values of the spin moment projections is reflected in the third term of the PAM Hamiltonian, where $\hat{n}_{f\sigma} = c^+_{k\sigma}c_{k\sigma}$ is the number operator of f electrons with the spin moment projection σ and U is the Hubbard repulsion energy. Finally, the last term in (1) describes hybridization processes of the collectivized and localized electrons with the corresponding rate determined by the matrix element V_k.

In what follows, we restrict ourself to considering the regime of strong correlations, assuming that the localized level E_0 is located within the lower half of the conductance band and $E_0 + U$ is above the conductance band top. If $U \gg |V_k|$, then introducing the atomic representation for localized f-ion states allows separating the high-energy hybridization processes from the low-energy ones. The former processes involve transitions of f ions into doubly occupied states, whose energy is determined by the large quantity U. Taking such transfers into account via the perturbation theory leads to an effective Hamiltonian involving an exchange coupling of spin moments of the collectivized and localized electrons and the exchange interaction between spin moments of f ions [22]. It then follows that the description of the physical properties of HF AFM intermetallides is realized in the framework of the modified Anderson Hamiltonian whose Wannier representation has the form

$$\widehat{\mathscr{H}} = \sum_{f\sigma}(\varepsilon - 2\sigma\mu_{\rm B}H - \mu)c^+_{f\sigma}c_{f\sigma} + \sum_{ff'\sigma} t_{ff'}c^+_{f\sigma}c_{f'\sigma} + \sum_{f\sigma}(E_\sigma - \mu)X^{\sigma\sigma}_f + \widehat{\mathscr{H}}_{\rm mix} + \widehat{\mathscr{H}}_{\rm exch}, \tag{2}$$

where

$$\widehat{\mathscr{H}}_{\rm mix} = \sum_{ff'\sigma}\{V_{ff'}c^+_{f\sigma}X^{0\sigma}_{f'} + \text{c.c.}\}, \qquad \widehat{\mathscr{H}}_{\rm exch} = \sum_{ff'} J_{ff'}(\vec{S}_f\vec{\sigma}_{f'}) - \frac{1}{2}\sum_{ff'} I_{ff'}(\vec{S}_f\vec{S}_{f'}).$$

In these expressions, $\varepsilon_\sigma = \varepsilon - 2\sigma\mu_{\rm B}H$ is the diagonal part of the collectivized state energy in a magnetic field in the Wannier representation, ε is the bare level of that energy, and $t_{ff'}$ are matrix elements that express the hopping rate of collectivized electrons from the site f to the site f' and are related to the energy ε_k by the standard Fourier transformation. The f-ion states are described in the atomic representation using the Hubbard operators $X^{m,n}_f = |m\rangle\langle n|$. The vector $|n\rangle$ describes a state with no electrons for $n = 0$ and a one-electron state with the spin moment projection σ for $n = \sigma$ ($\sigma = \uparrow, \downarrow$). States with two on-site f electrons are not involved in the formation of the Hilbert space of effective Hamiltonian (2), because the processes involving doubly occupied states are taken into account perturbatively. This is also the reason for the term $\widehat{\mathscr{H}}_{\rm exch}$ in (2), which accounts for the s–f-exchange interaction between spin moments of localized and collectivized electrons and also the exchange interaction in the localized subsystem, with the respective exchange integrals $J_{ff'}$ and $I_{ff'}$. The behavior of these integrals under a change in hybridization and in the distance between lattice sites was analyzed in [22]. Also because of the above reason, the operator $\widehat{\mathscr{H}}_{\rm mix}$ takes only the low-energy hybridization process between localized and collectivized states into account with the hybridization parameter $V_{ff'}$.

The components of the localized quasispin operators $\vec{S}_f$ are related to the Hubbard operators as

$$\begin{aligned} &S^x_f = \frac{1}{2}\sum_\sigma X^{\sigma\bar\sigma}_f, \qquad S^y_f = i\sum_\sigma \sigma X^{\bar\sigma\sigma}_f, \qquad S^z_f = \sum_\sigma \sigma X^{\sigma\sigma}_f, \\ &S^+_f = X^{\uparrow\downarrow}_f, \qquad\qquad S^-_f = X^{\downarrow\uparrow}_f, \qquad\qquad \bar\sigma = -\sigma. \end{aligned} \tag{3}$$

For collectivized states, we use the usual relation of the spin operator components to Fermi operators:

$$\sigma^x_f = \frac{c^+_{f\uparrow}c_{f\downarrow} + c^+_{f\downarrow}c_{f\uparrow}}{2}, \qquad \sigma^y_f = \frac{c^+_{f\uparrow}c_{f\downarrow} - c^+_{f\downarrow}c_{f\uparrow}}{2i}, \qquad \sigma^z_f = \frac{c^+_{f\uparrow}c_{f\uparrow} - c^+_{f\downarrow}c_{f\downarrow}}{2}.$$

In describing the canted AFM phase, as usual, we introduce two sublattices F and G. In what follows, the indices f and g denote sites belonging to the respective sublattices F and G. Then the Hamiltonian describing noninteracting collectivized and localized electrons can be written as

$$\begin{aligned} \widehat{\mathscr{H}}_0 = &\sum_{f\sigma}(\varepsilon_\sigma - \mu)c^+_{f\sigma}c_{f\sigma} + \sum_{g\sigma}(\varepsilon_\sigma - \mu)a^+_{g\sigma}a_{g\sigma} + \sum_{f\sigma}(E_\sigma - \mu)X^{\sigma\sigma}_f + \sum_{g\sigma}(E_\sigma - \mu)X^{\sigma\sigma}_g + \\ &+ \sum_{ff'\sigma} t_{ff'}c^+_{f\sigma}c_{f'\sigma} + \sum_{gg'\sigma} t_{gg'}a^+_{g\sigma}a_{g'\sigma} + \sum_{fg\sigma} t_{fg}(a^+_{g\sigma}c_{f\sigma} + c^+_{f\sigma}a_{g\sigma}), \end{aligned} \tag{4}$$

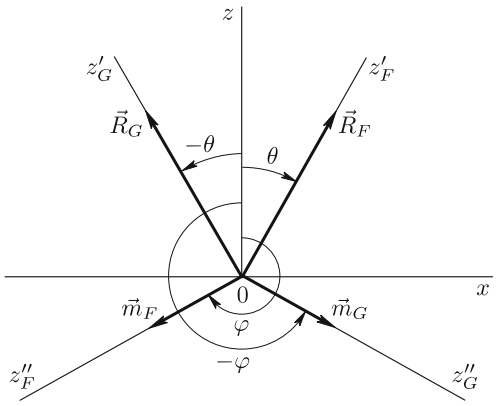

Fig. 1. Direction of the magnetization vectors in the canted phase: the magnetic field is directed along the z axis.

where the notation for the creation and annihilation operators for conductance electrons pertaining to the sublattice G is changed to a_g^+ and a_g. The previous notation is kept for the F-sublattice operators. The third and fourth terms in (4) reflect the contributions of localized states of the respective sublattices F and G. The fifth and sixth terms respectively describe the hopping of conductance electrons inside the sublattices F and G, and the seventh term describes hopping between the sublattices.

It is useful to represent the term $\widehat{\mathscr{H}}_{\rm mix}$ in the Hamiltonian in the two-sublattice description as

$$\widehat{\mathscr{H}}_{\rm mix} = \sum_{fg\sigma}(W_{fg}c^+_{f\sigma}X^{0\sigma}_g + W_{gf}a^+_{g\sigma}X^{0\sigma}_f) + \sum_{ff'\sigma} V_{ff'}c^+_{f\sigma}X^{0\sigma}_{f'} + \sum_{gg'\sigma} V_{gg'}a^+_{g\sigma}X^{0\sigma}_{g'} + \{\text{c.c.}\}, \tag{5}$$

where the first sum describes hybridization processes between states of different sublattices. To describe the rate of such processes, we introduce the new notation W_{fg}. Hybridization processes within one sublattice are reflected in the second and third terms, where the previous notation for the matrix elements is kept.

After the partition into sublattices, the exchange part of the Hamiltonian can be written as

$$\begin{aligned}\widehat{\mathscr{H}}_{\rm exch} = &\sum_{ff'} J_{ff'}(\vec{S}_f\vec{\sigma}_{f'}) + \sum_{gg'} J_{gg'}(\vec{S}_g\vec{\sigma}_{g'}) + \sum_{fg} L_{fg}(\vec{S}_f\vec{\sigma}_g + \vec{S}_g\vec{\sigma}_f) - \\ &- \frac{1}{2}\sum_{ff'} I_{ff'}(\vec{S}_f\vec{S}_{f'}) - \frac{1}{2}\sum_{gg'} I_{gg'}(\vec{S}_g\vec{S}_{g'}) + \sum_{fg} K_{fg}(\vec{S}_f\vec{S}_g).\end{aligned} \tag{6}$$

As in the preceding expressions, the old notation is kept here for interactions within one sublattice. Matrix elements for the s–f-exchange interaction of distinct sublattices are denoted differently by L_{fg}. A different designation K_{fg} is also used for the exchange integrals between localized spin moments of distinct sublattices. That such notational changes are necessary becomes clear in what follows.

3. Unitary transformation of the canted-phase Hamiltonian and equations for the angular direction of equilibrium magnetizations

Recalling that magnetic sublattices experience a canting in an external magnetic field in the AFM phase (see Fig. 1), we introduce four local coordinate systems such that their quantization axes (the new Oz axes) are directed the same as the equilibrium magnetizations $\vec{R}_F$ and $\vec{R}_G$ of localized and $\vec{m}_F$ and $\vec{m}_G$ of collectivized electrons in the sublattices F and G. We emphasize that in the considered noncollinear

geometry, the magnetization vectors $\vec{m}_F$ and $\vec{m}_G$ of the collectivized electron sublattices are not necessarily oriented parallel or antiparallel to the vectors $\vec{R}_F$ and $\vec{R}_G$. But the effect of the canting of magnetic moments of the collectivized subsystem cannot be neglected because, as can be seen from numerical analysis, that can lead, for example, to negative values of heat capacity. The passage to the local axes is performed by rotations about the Oy axis of the original coordinate systems for each of the four magnetic subsystems through the angles θ, $-\theta$, φ, and $-\varphi$. The angles θ and $-\theta$ are assumed to characterize the respective deviations of the localized magnetization direction in the sublattices F and G from the original Oz axis in the Oxz plane. Similarly, the angles φ and $-\varphi$ specify the orientation of the collectivized magnetization in the sublattices F and G. The above passage to local axes corresponds to unitarily transforming the Hamiltonian as

$$\widehat{\mathscr{H}} \to \widetilde{\widehat{\mathscr{H}}} = U(\theta,\varphi)\cdot\widehat{\mathscr{H}}\cdot U^{+}(\theta,\varphi) \tag{7}$$

with the unitary operator

$$U(\theta,\varphi) = \prod_f \prod_g \exp\{i(\theta S_f^y + \varphi\sigma_f^y)\}\exp\{-i(\theta S_g^y + \varphi\sigma_g^y)\}. \tag{8}$$

Using expression (8), we find the transformation laws for the operators pertaining to the sublattice F:

$$\begin{aligned}
c_{f\sigma}(\varphi) &= U c_{f\sigma} U^{+} = c_{f\sigma}\cos\frac{\varphi}{2} - 2\sigma c_{f\bar{\sigma}}\sin\frac{\varphi}{2},\\
X_f^{0\sigma}(\theta) &= U X_f^{0\sigma} U^{+} = X_f^{0\sigma}\cos\frac{\theta}{2} - 2\sigma X_f^{0\bar{\sigma}}\sin\frac{\theta}{2},\\
X_f^{\sigma\sigma}(\theta) &= U X_f^{\sigma\sigma} U^{+} = \frac{1}{2}\sum_{\sigma_1} X_f^{\sigma_1\sigma_1} - \sigma\sin\theta\sum_{\sigma_1} X_f^{\sigma_1\bar{\sigma}_1} + 2\sigma\cos\theta\sum_{\sigma_1}\sigma_1 X_f^{\sigma_1\sigma_1}.
\end{aligned} \tag{9}$$

The spin operators of localized electrons of the sublattice F transform as

$$\begin{aligned}
S_f^x(\theta) &\equiv U S_f^x U^{+} = S_f^x\cos\theta + S_f^z\sin\theta, \qquad & \sigma_f^x(\varphi) &\equiv U\sigma_f^x U^{+} = \sigma_f^x\cos\varphi + \sigma_f^z\sin\varphi,\\
S_f^y(\theta) &\equiv U S_f^y U^{+} = S_f^y, & \sigma_f^y(\varphi) &\equiv U\sigma_f^y U^{+} = \sigma_f^y,\\
S_f^z(\theta) &\equiv U S_f^z U^{+} = S_f^z\cos\theta - S_f^x\sin\theta, \qquad & \sigma_f^z(\varphi) &\equiv U\sigma_f^z U^{+} = \sigma_f^z\cos\varphi - \sigma_f^x\sin\varphi.
\end{aligned} \tag{10}$$

The transformation laws for the G-sublattice operators $a_{g\sigma}$, $X_g^{0\sigma}$, $X_g^{\sigma\sigma}$, $\vec{S}_g$, and $\vec{\sigma}_g$ follow from Eqs. (9) and (10) by replacing the indices f with g and the angles θ and φ with $-\theta$ and $-\varphi$.

Using formulas (9) and (10), we find the terms of the transformed Hamiltonian:

$$\begin{aligned}
\widehat{\mathscr{H}}_0 = {} & \sum_{k\sigma}(t_k - 2\sigma\mu_{\mathrm{B}}H\cos\varphi - \mu)(c_{k\sigma}^{+}c_{k\sigma} + a_{k\sigma}^{+}a_{k\sigma}) - 2\mu_{\mathrm{B}}H\sin\varphi\Big(\sum_g\sigma_g^x - \sum_f\sigma_f^x\Big) +\\
& + \sum_{k\sigma}[\Gamma_k\cos\varphi(c_{k\sigma}^{+}a_{k\sigma} + a_{k\sigma}^{+}c_{k\sigma}) + \Gamma_k 2\sigma\sin\varphi(c_{k\sigma}^{+}a_{k\bar{\sigma}} + a_{k\bar{\sigma}}^{+}c_{k\sigma})] +\\
& + (E_0 - \mu - g\sigma\mu_{\mathrm{B}}H\cos\theta)\Big(\sum_{f\sigma}X_f^{\sigma\sigma} + \sum_{g\sigma}X_g^{\sigma\sigma}\Big) +\\
& + g\mu_{\mathrm{B}}H\sin\theta\Big(\sum_f S_f^x - \sum_g S_g^x\Big).
\end{aligned} \tag{11}$$

In writing the kinetic energy, we pass to the quasimomentum representation, defining the Brillouin zone with the two-sublattice structure taken into account. Accordingly, the Fourier transforms of the hopping integrals are separated into intra- and inter-sublattice ones:

$$t_{ff'} = \frac{1}{N}\sum_k e^{ik(f-f')}t_k, \qquad t_{fg} = \frac{1}{N}\sum_k e^{ik(f-g)}\Gamma_k, \tag{12}$$

where N is the number of sites in a sublattice.

After unitary transformation (7), operator (5) becomes

$$\begin{aligned}
\widehat{\mathscr{H}}_{\rm mix} = \sum_{fg\sigma}\Bigg\{ & W_{fg}\Bigg[c^+_{f\sigma}X^{0\sigma}_g\cos\left(\frac{\varphi+\theta}{2}\right) + 2\sigma c^+_{f\sigma}X^{0\bar\sigma}_g\sin\left(\frac{\varphi+\theta}{2}\right) + \\
& + a^+_{g\sigma}X^{0\sigma}_f\cos\left(\frac{\varphi+\theta}{2}\right) - 2\sigma a^+_{g\sigma}X^{0\bar\sigma}_f\sin\left(\frac{\varphi+\theta}{2}\right)\Bigg] + \text{c.c.}\Bigg\} + \\
& + \sum_{ff'\sigma} V_{ff'}\left[c^+_{f\sigma}X^{0\sigma}_{f'}\cos\left(\frac{\varphi-\theta}{2}\right) + 2\sigma c^+_{f\sigma}X^{0\bar\sigma}_{f'}\sin\left(\frac{\varphi-\theta}{2}\right) + \text{c.c.}\right] + \\
& + \sum_{gg'\sigma} V_{gg'}\left[a^+_{g\sigma}X^{0\sigma}_{g'}\cos\left(\frac{\varphi-\theta}{2}\right) - 2\sigma a^+_{g\sigma}X^{0\bar\sigma}_{g'}\sin\left(\frac{\varphi-\theta}{2}\right) + \text{c.c.}\right].
\end{aligned} \tag{13}$$

For the exchange part of the Hamiltonian, we obtain

$$\begin{aligned}
\widehat{\mathscr{H}}_{\rm exch} = & \sum_{ff'} J_{ff'}[S^y_f\sigma^y_{f'} + (S^x_f\sigma^x_{f'} + S^z_f\sigma^z_{f'})\cos(\varphi-\theta) + (S^x_f\sigma^z_{f'} - S^z_f\sigma^x_{f'})\sin(\varphi-\theta)] + \\
& + \sum_{gg'} J_{gg'}[S^y_g\sigma^y_{g'} + (S^x_g\sigma^x_{g'} + S^z_g\sigma^z_{g'})\cos(\varphi-\theta) - (S^x_g\sigma^z_{g'} - S^z_g\sigma^x_{g'})\sin(\varphi-\theta)] + \\
& + \sum_{fg} L_{fg}[S^y_f\sigma^y_g + (S^x_f\sigma^x_g + S^z_f\sigma^z_g)\cos(\varphi+\theta) + (S^z_f\sigma^x_g - S^x_f\sigma^z_g)\sin(\varphi+\theta) + \\
& + S^y_g\sigma^y_f + (S^x_g\sigma^x_f + S^z_g\sigma^z_f)\cos(\varphi+\theta) - (S^z_g\sigma^x_f - S^x_g\sigma^z_f)\sin(\varphi+\theta)\big] - \\
& - \frac{1}{2}\sum_{ff'} I_{ff'}(\vec S_f\vec S_{f'}) - \frac{1}{2}\sum_{gg'} I_{gg'}(\vec S_g\vec S_{g'}) + \\
& + \sum_{fg} K_{fg}[(S^x_gS^x_f + S^z_gS^z_f)\cos 2\theta + (S^x_gS^z_f - S^z_gS^x_f)\sin 2\theta + S^y_fS^y_g].
\end{aligned} \tag{14}$$

We derive equations for the equilibrium values of the angles θ and φ in the approximation where spin fluctuation contributions are assumed to be negligibly small. Because the equilibrium magnetization vectors must be oriented along their quantization axes in local coordinate systems, it follows that in the considered approximation, the vanishing requirement for expressions linear in the operators S^x_f, S^x_g, σ^x_f, and σ^x_g leads to the system of equations

$$\begin{aligned}
& 2\mu_{\rm B}H\sin\varphi - R(J_0\sin(\varphi-\theta) + L_0\sin(\varphi+\theta)) = 0, \\
& g\mu_{\rm B}H\sin\theta + m(J_0\sin(\varphi-\theta) - L_0\sin(\varphi+\theta)) - RK_0\sin 2\theta = 0.
\end{aligned} \tag{15}$$

Here, we introduce the notation $R = \langle S^z_f\rangle = \langle S^z_g\rangle$, $m = \langle\sigma^z_f\rangle = \langle\sigma^z_g\rangle$, and I_0 is the Fourier transform of the exchange integral at $q = 0$. The quantities K_0, J_0, and L_0 are understood similarly.

System of equations (15) has the trivial solution $\theta = 0$, $\varphi = 0, \pi$, which corresponds to the state where localized magnetizations of the sublattices F and G are oriented along the original Oz axis (this occurs in strong magnetic fields for an AFM system); the magnetization vector of collectivized electrons is then oriented parallel ($\varphi = 0$) or antiparallel ($\varphi = \pi$) to the localized magnetization.

For $\theta \neq 0$, solving system (15) amounts to finding the solution of a single equation for the equilibrium angle θ,

$$(g\mu_{\rm B}H - 2K_0R\cos\theta)\big[R^2(J_0 - L_0)^2\sin^2\theta + \big((J_0 + L_0)R\cos\theta - 2\mu_{\rm B}H\big)^2\big] = \\ = m^2[4J_0L_0R\cos\theta - 2\mu_{\rm B}H(J_0 + L_0)]^2. \qquad (16)$$

The angle φ is then calculated in terms of the found θ as

$$\cot\varphi = \frac{2\mu_{\rm B}H - R(J_0 + L_0)\cos\theta}{R(L_0 - J_0)\sin\theta}. \qquad (17)$$

4. Slave-boson representation and a quadratic form of the fermion subsystem

It is known that the auxiliary (slave) boson representation for Hubbard operators [10] can be used to find the spectrum of Fermi excitations in the approximation where relaxation processes are ignored. This representation has proved quite effective in understanding the nature of HF formation in nonmagnetic intermetallides. In the two-sublattice case, this representation is written as

$$X_f^{0\sigma} = e_f^+ d_{f\sigma}, \qquad X_f^{\sigma_1\sigma_2} = d_{f\sigma_1}^+ d_{f\sigma_2}, \qquad X_g^{0\sigma} = e_g^+ b_{g\sigma}, \qquad X_g^{\sigma_1\sigma_2} = b_{g\sigma_1}^+ b_{g\sigma_2}, \qquad (18)$$

where the Bose operators e_f^+ and e_f create and annihilate a state with no electrons at the site f and the creation and annihilation operators of localized electrons at the site f or g are respectively denoted by $d_{f\sigma}^+$ and $d_{f\sigma}$ or $b_{g\sigma}^+$ and $b_{g\sigma}$. Nonphysical states are eliminated by the constraints

$$e_f^+ e_f + \sum_\sigma d_{f\sigma}^+ d_{f\sigma} = 1, \qquad e_g^+ e_g + \sum_\sigma b_{g\sigma}^+ b_{g\sigma} = 1. \qquad (19)$$

In the mean field approach, the totality of local constraints is replaced with global constraints, under the assumption that the slave bosons constitute a condensate phase and the Bose operators can be replaced with their means $e_0 = \langle e_f^+\rangle = \langle e_f\rangle = \langle e_g^+\rangle = \langle e_g\rangle$, as in the theory of a weakly nonideal Bose liquid for bosons with zero quasimomentum. Accordingly, the above restrictions become

$$e_0^2 + \sum_\sigma n_{f\sigma} = 1, \qquad e_0^2 + \sum_\sigma n_{g\sigma} = 1, \qquad (20)$$

where $n_{f\sigma} = n_{g\sigma}$ is the number of spin-σ localized electrons per lattice site. In what follows, as usual, condition (20) is taken into account by introducing a Lagrange multiplier λ.

We introduce the two-component operators in the quasimomentum representation

$$c_k^+ \equiv (c_{k\uparrow}^+, c_{k\downarrow}^+), \qquad a_k^+ \equiv (a_{k\uparrow}^+, a_{k\downarrow}^+), \qquad b_k^+ \equiv (b_{k\uparrow}^+, b_{k\downarrow}^+), \qquad d_k^+ \equiv (d_{k\uparrow}^+, d_{k\downarrow}^+) \qquad (21)$$

and construct the block operator $A_k^+ = (c_k^+, a_k^+, b_k^+, d_k^+)$. The Hamiltonian is then written as

$$\widehat{\mathscr{H}} = \sum_k A_k^+ \widehat{M}_k(\varphi,\theta) A_k + R^2N(I_0 - K_0\cos 2\theta) - 2NRmh_z + 2\lambda N(e_0^2 - 1), \qquad (22)$$

where the eight-dimensional matrix $\widehat{M}_k(\varphi,\theta)$ is defined in block form as

$$\widehat{M}_k(\varphi,\theta)=\begin{pmatrix} \widehat{T}_k & \widehat{\Gamma}_k(\varphi) & \widehat{W}_k(\varphi+\theta) & \widehat{V}_k(\varphi-\theta) \\ \widetilde{\widehat{\Gamma}}_k(\varphi) & \widehat{T}_k & \widetilde{\widehat{V}}_k(\varphi-\theta) & \widetilde{\widehat{W}}_k(\varphi+\theta) \\ \widetilde{\widehat{W}}^*_k(\varphi+\theta) & \widehat{V}^*_k(\varphi-\theta) & \hat{L} & 0 \\ \widetilde{\widehat{V}}^*_k(\varphi-\theta) & \widehat{W}^*_k(\varphi+\theta) & 0 & \hat{L} \end{pmatrix}, \tag{23}$$

where the tilde denotes transposition and the star denotes Hermitian conjugation. The second-order matrices involved in $\widehat{M}_k(\varphi,\theta)$ are given by

$$\widehat{\Gamma}_k(\varphi)=\Gamma_k\widehat{P}(\varphi), \qquad \widehat{W}_k(\varphi+\theta)=e_0W_k\widehat{P}\biggl(\frac{\varphi+\theta}{2}\biggr),$$

$$\widehat{V}_k(\varphi-\theta)=e_0V_k\widehat{P}\biggl(\frac{\varphi-\theta}{2}\biggr), \qquad \widehat{P}(\chi)=\begin{pmatrix} \cos\chi & \sin\chi \\ -\sin\chi & \cos\chi \end{pmatrix},$$

$$\widehat{T}_k=\begin{pmatrix} \xi_k-\dfrac{\bar{H}_c}{2} & 0 \\ 0 & \xi_k+\dfrac{\bar{H}_c}{2} \end{pmatrix}, \qquad \hat{L}=\begin{pmatrix} \zeta-\dfrac{\bar{H}_d}{2} & 0 \\ 0 & \zeta+\dfrac{\bar{H}_d}{2} \end{pmatrix},$$

where $\xi_k=t_k-\mu$, $\zeta=E_0-\mu+\lambda$, and $\bar{H}_c=2\mu_{\mathrm{B}}H\cos\varphi-Rh_z$ and $\bar{H}_d=g\mu_{\mathrm{B}}H\cos\theta-mh_z-R(K_0\cos2\theta-I_0)$ define the respective effective fields acting on the spin variables of the collectivized and localized subsystems. Here, $h_z=J_0\cos(\varphi-\theta)+L_0\cos(\varphi+\theta)$. The functions V_k and W_k are defined in terms of Fourier transformations of intra- and inter-sublattice hybridization parameters in the Wannier representation:

$$V_k=\sum_{f-f'}e^{-ik(f-f')}V(f-f'), \qquad W_k=\sum_{f-g}e^{-ik(f-g)}W(f-g).$$

When the slave-boson description of HFs is used, the energy of the localized level is standardly renormalized via the additive shift by the Lagrange multiplier [10]. The use of this representation also underlies the appearance of the last term in (22).

It follows from the presented structure of the Hamiltonian that the problem noncollinearity due to hybridization processes between collectivized and localized electrons leads to a mixing of states of the different spin subbands. This results in a high sensitivity of the electronic characteristics of the system to the external magnetic field, which changes the orientation of magnetic sublattices and therefore modulates the rate of hybridization processes of mixing of the electron subsystems.

We proceed with solving the problem by diagonalizing the eighth-order form and calculating self-consistent fields and the renormalization parameters λ and e_0.

5. Green's functions and the dispersion equation

To find the spectrum and the thermodynamic averages, we use the method of two-time retarded Green's functions [23]. Introducing the vector function

$$\langle\langle A_k(t)|c^+_{k\sigma}(t')\rangle\rangle=-i\theta(t-t')\langle[A_k(t),c^+_{k\sigma}(t')]_+\rangle, \tag{24}$$

we write its equation of motion in the (k,ω) representation:

$$(\omega\cdot\hat{I}-\widehat{M}_k(\varphi,\theta))\langle\langle A_k|c^+_{k\sigma}\rangle\rangle_\omega=B_\sigma, \tag{25}$$

where $B_\sigma = \langle\{A_k, c^+_{k\sigma}\}_+\rangle$ and $\hat{I}$ is the eight-dimensional unit matrix. The problem is essentially simplified by using the unitary transformation

$$\widehat{U}_8 = \frac{1}{2}\begin{pmatrix} \hat{\eta}_1 & \hat{\eta}_1^* & \hat{\eta}_1^* & -\hat{\eta}_1 \\ \hat{\eta}_1^* & \hat{\eta}_1 & -\hat{\eta}_1 & \hat{\eta}_1^* \\ \hat{\eta}_2^* & \hat{\eta}_2 & -\hat{\eta}_2 & \hat{\eta}_2^* \\ \hat{\eta}_2 & \hat{\eta}_2^* & \hat{\eta}_2^* & -\hat{\eta}_2 \end{pmatrix}, \qquad \hat{\eta}_1 = \begin{pmatrix} 1 & 0 \\ i & 0 \end{pmatrix}, \qquad \hat{\eta}_2 = \begin{pmatrix} 0 & 1 \\ 0 & i \end{pmatrix}, \tag{26}$$

which reduces the eighth-order matrix in (25) to a matrix of block-diagonal form:

$$\widehat{U}_8^+ \cdot (\omega \cdot \hat{I} - \widehat{M}_k(\varphi,\theta)) \cdot \widehat{U}_8 = \begin{pmatrix} \widehat{M}^{(4)}_{k,+1/2} & 0 \\ 0 & \widehat{M}^{(4)}_{k,-1/2} \end{pmatrix}, \qquad \widehat{M}^{(4)}_{k,s} = \begin{pmatrix} \widehat{\Omega}^{(2)}_s & \widehat{H}^{(2)}_s \\ (\widehat{H}^{(2)}_s)^\dagger & \widehat{\Omega}^{(2)}_{-s} \end{pmatrix}. \tag{27}$$

The second-order matrices through which the $M^{(4)}_{k,s}$ are expressed are given by ($s = \pm 1/2$)

$$\begin{aligned} \widehat{\Omega}^{(2)}_s &= \begin{pmatrix} \omega - \xi_k & -e_0 V_k e^{is(\varphi-\theta)} \\ -e_0 V_k^* e^{-is(\varphi-\theta)} & \omega - \zeta \end{pmatrix}, \\ \widehat{H}^{(2)}_s &= \begin{pmatrix} s\bar{H}_c - \Gamma_k e^{i2s\varphi} & -e_0 W_k e^{is(\varphi+\theta)} \\ -e_0 W_k^* e^{is(\varphi+\theta)} & s\bar{H}_d \end{pmatrix}. \end{aligned} \tag{28}$$

Finding the spectrum now amounts to solving two dispersion equations

$$\begin{aligned} D^{(4)}_{k,s}(\omega) = &\left[(\omega-\zeta)^2 - \frac{\bar{H}_d^2}{4}\right]\left[(\omega-\xi_k)^2 - \Gamma_k^2 - \frac{\bar{H}_c^2}{4} + 2s\bar{H}_c\Gamma_k\cos\varphi\right] + \\ &+ 2(\omega-\zeta)[u_k^2(s\bar{H}_c\cos\varphi - \Gamma_k) - v_k^2(\omega-\xi_k)] - u_k^4 + v_k^4 + \\ &+ \bar{H}_d\Big[2s\cos\theta(u_k^2(\omega-\xi_k) + v_k^2\Gamma_k) - \\ &- \frac{1}{2}\bar{H}_c(|\widetilde{W}_k|^2\cos(\varphi+\theta) + |\widetilde{V}_k|^2\cos(\varphi-\theta))\Big] = 0 \end{aligned} \tag{29}$$

for each value of the quantum number s. We here use the notation

$$v_k^2 = |\widetilde{V}_k|^2 + |\widetilde{W}_k|^2, \qquad u_k^2 = \widetilde{V}_k^*\widetilde{W}_k + \widetilde{V}_k\widetilde{W}_k^*, \qquad \widetilde{V}_k = e_0 V_k, \qquad \widetilde{W}_k = e_0 W_k. \tag{30}$$

In the limit case $V_k = W_k = 0$, the dispersion equation takes the obvious form

$$\left[(\omega-\zeta)^2 - \frac{\bar{H}_d^2}{4}\right]\left[(\omega-\xi_k)^2 - \Gamma_k^2 - \frac{\bar{H}_c^2}{4} + 2s\bar{H}_c\Gamma_k\cos\varphi\right] = 0. \tag{31}$$

Its solutions

$$\omega = \zeta \pm s\bar{H}_d, \qquad \omega = \xi_k \pm \sqrt{\Gamma_k^2 + \frac{\bar{H}_c^2}{4} - 2s\bar{H}_c\Gamma_k\cos\varphi} \tag{32}$$

describe a localized level and the band spectrum of collectivized electrons placed into a field modulated by the AFM structure and split with respect to the spin variable s by the effective fields $\bar{H}_c$ and $\bar{H}_d$.

6. Self-consistency equations

To describe the system thermodynamically, we must use seven self-consistency equations. The first five are for (1) the chemical potential μ at a fixed electron concentration n, (2) the Lagrange multiplier λ, (3) the mean number of auxiliary bosons e_0, and (4 and 5) the equilibrium values of the magnetizations of localized (R) and collectivized (m) subsystems. They can be written as

$$n = \frac{2}{N}\left(\sum_{k\sigma}\langle c^+_{k\sigma}c_{k\sigma}\rangle + \sum_{k\sigma}\langle d^+_{k\sigma}d_{k\sigma}\rangle\right), \qquad -2\lambda e_0^2 = \frac{1}{N}\sum_k[\langle c^+_k(\widehat{W}_k b_k + \widehat{V}_k d_k)\rangle + \text{c.c.}],$$
$$e_0^2 = 1 - \frac{1}{N}\sum_{k\sigma}\langle d^+_{k\sigma}d_{k\sigma}\rangle, \qquad R = \frac{1}{N}\sum_{k\sigma}\sigma\langle d^+_{k\sigma}d_{k\sigma}\rangle, \qquad m = \frac{1}{N}\sum_{k\sigma}\sigma\langle c^+_{k\sigma}c_{k\sigma}\rangle. \tag{33}$$

Two equations for the canting angles φ and θ of the magnetic sublattices are written above, Eq. (15). In deriving these expressions, we use the equivalence of the sublattices F and G.

Using the spectral theorem, in particular, we obtain

$$\langle c^+_{k\sigma}c_{k\sigma}\rangle = \frac{1}{2}\sum_{j=1}^{4}\left\{\frac{A^{(cc)}_{\sigma\sigma}(k, E^{(j)}_{k\bar\sigma})f(E^{(j)}_{k\bar\sigma} - \mu)}{\prod'_l(E^{(j)}_{k\bar\sigma} - E^{(l)}_{k\bar\sigma})} + \frac{B^{(cc)}_{\sigma\sigma}(k, E^{(j)}_{k\sigma})f(E^{(j)}_{k\sigma} - \mu)}{\prod'_l(E^{(j)}_{k\sigma} - E^{(l)}_{k\sigma})}\right\}. \tag{34}$$

For a fixed σ, the energies $E^{(j)}_{k\sigma}$, $j = 1, \ldots, 4$, are solutions of dispersion equation (29). The prime on the product signs in the denominators in (34) indicates the absence of the factor with $l = j$. Expressions for the functions $A^{(cc)}_{\sigma\sigma}(k, E^{(j)}_{k\bar\sigma})$ and $B^{(cc)}_{\sigma\sigma}(k, E^{(j)}_{k\sigma})$ are given in the appendix. The other correlation functions in the self-consistency equations are calculated similarly. After the correlation functions are substituted in the self-consistency equations (see the appendix), we obtain closed equations describing the thermodynamic properties of an AFM HF system in an external magnetic field.

7. Effect of the canting of magnetic sublattices on the HF energy spectrum

It was assumed in numerical computations that the atom ordering corresponds to a body-centered cubic lattice and that the energy structure of band electrons is formed due to electron hopping only between the nearest neighbors. The hopping rate is denoted by t'. The Fourier transform corresponding to hopping within one sublattice is then equal to zero ($t_k = 0$), and the Fourier transform of inter-sublattice hopping parameters is given by

$$\Gamma_k = 8t'\cos\left(\frac{k_x b}{2}\right)\cos\left(\frac{k_y b}{2}\right)\cos\left(\frac{k_z b}{2}\right), \tag{35}$$

where b is the magnetic cell parameter. It was also assumed for simplicity that the hybridization and s–f-exchange processes between f- and s-electron states are realized only if these states belong to the same Wannier cell. Then $V_q = V$, $W_q = 0$, $J_q = J$, and $L_q = 0$, where V and J are the respective values of the hybridization parameter and the s–f-exchange integral. The exchange interaction in the subsystem of localized electrons was taken into account only between the nearest spin moments. Hence, $I_q = 0$ and $K_q = 8K_1\cos(q_x b/2)\cos(q_y b/2)\cos(q_z b/2)$, where K_1 is the exchange integral for nearest neighbors. In what follows, all the energy parameters are measured in units of $|t'|$, $t' < 0$.

We begin analyzing solutions of the system of self-consistency equations with the case $H = 0$. In Fig. 2, we show the structure of the original Fermi spectrum in the collinear AFM phase without taking the hybridization processes into account. The dependence of energy on quasimomentum, $E^{(j)}_{ks}$, $j = 1, 2, 3, 4$, is shown in the right part of Fig. 2 for $s = +1/2$ and in the left part for $s = -1/2$. It can be seen that all four branches of the spectrum are degenerate with respect to the quantum number s (the left

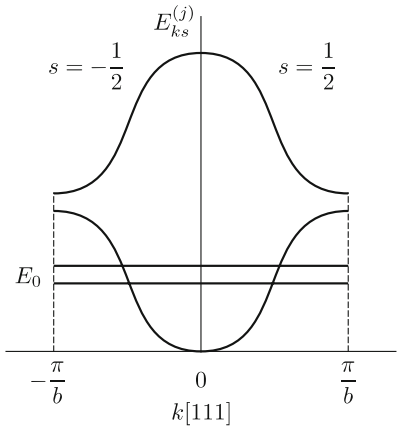

Fig. 2. The original PAM band structure in the AFM phase at $H = 0$ and $V = 0$.

and right branches in the figure are identical). The doubling is related to the AFM structure: a twofold reduction in the Brillouin zone and the corresponding increase in the number of branches compared with the paramagnetic case. The quasimomentum variation is chosen along the direction [111]. For the other directions, the qualitative picture is the same. The straight lines correspond to the localized states of the f subsystem with the energy E_0 split by the exchange field $\bar{H}_d$. Dispersion lines reflect the bare spectrum of collectivized electrons in the AFM phase.

In what follows, we also restrict ourself to the case where the localized level is in the lower half of the conductance band (see Fig. 2) and the chemical potential is located in its immediate vicinity (the HF regime). Because the effective field $\bar{H}_d$ that defines the splitting energy of f states is much less than the conductance band width, the leading changes in the energy spectrum associated with turning on the hybridization processes and the canting of magnetic sublattices occur in the immediate vicinity of E_0. With this in mind, in expounding the results of the self-consistent computation, we focus only on the modification of the Fermi spectrum in the above energy domain. We also note that at the chosen value of the chemical potential, the top branches of the spectrum with $j = 4$ do not contribute to the thermodynamic properties of the system.

In Fig. 3a, the quasiparticle spectrum evaluated in the neighborhood of the localized level is shown for the AFM phase ($H = 0$). The computation was performed at the model parameter values $E_0 = -4$, $V = 0.4$, $K_0 = 0.02$, $J_0 = 0.5$, and $n = 2.2$. The temperature was $T = 1\,\mathrm{K}$. The self-consistent value of the magnetic moment with the selected parameters was equal to $R = 0.381$. The main property of the obtained spectrum is the appearance of a narrow heavy-quasiparticle band separated by energy gaps from both below and above. This constitutes a difference of the obtained spectrum from the spectrum of heavy quasiparticles in the paramagnetic phase, where heavy-quasiparticle states are separated by a gap on only one side. The maximum width of the split HF band is of the order of $\bar{H}_d$ and is determined by the exchange parameters and by the values of magnetic moments of the localized and collectivized subsystems.

In Fig. 3b, the density $D_{f\sigma}(E)$ of states for localized electrons of the sublattice F is shown separately for each value of the variable σ characterizing the spin moment projection on the quantization axis z'_F (see Fig. 1). Comparing Figs. 3a and 3b shows that the horizontal parts of the spectrum formed in the neighborhood of the ex-bottom localized level describe ground-state f electrons with spins directed along the quantization axis z'_F ($\sigma =\uparrow$). Similarly, the horizontal parts of the spectrum in the neighborhood of the ex-top localized level pertain to f-electron states with the spin moments directed against the z'_F axis ($\sigma =\downarrow$). Because the position of the chemical potential μ is such that the f states with $\sigma =\uparrow$ are mainly filled, the ground state of the system is characterized by a long-range AFM order.

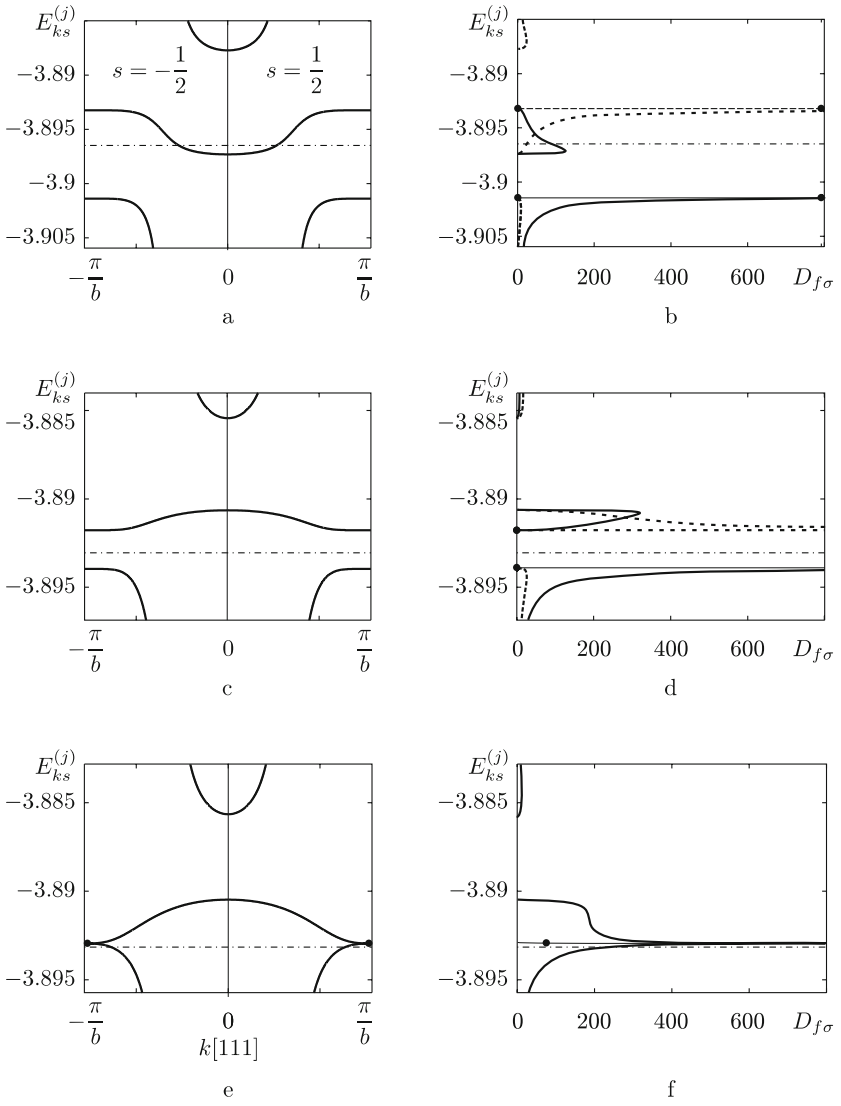

Fig. 3. Temperature evolution of the Fermi spectrum (a, c, e) and the density of localized electron states (b: $T = 1\,\mathrm{K}$ and $R = 0.381$; d: $T = 21\,\mathrm{K}$ and $R = 0.103$; f: $T = 23\,\mathrm{K}$ and $R = 0$) for the PAM in the collinear AFM phase ($H = 0$) in the neighborhood of the localized level E_0. The dash-dotted line shows the location of the chemical potential. In b, d, and f, the solid line corresponds to the density of f-electron states $D_{f\uparrow}$, and the dashed line corresponds to $D_{f\downarrow}$. For the selected parameters, the Néel temperature is $T_\mathrm{N} \approx 23\,\mathrm{K}$.

The evolution of the considered dispersion curves with respect to temperature is shown in Figs. 3c–3f. It can be seen that the width of the narrow band decreases as the temperature increases. At a temperature of the order of 19 K (the Néel temperature T_N of $PuGa_3$ is given by 24 K [2]), the narrow band degenerates into a level; as the temperature increases further, the band is inverted (Fig. 3c). As a result of the inversion, the maximum dispersion of the narrow band ($E_{ks}^{(2)}$) corresponds to states in the center of the Brillouin zone. We note that, importantly, as also for $T = 1\,\mathrm{K}$, a disproportion is still preserved in filling these states by localized electrons with different spin moment projections σ. For the narrow band ($j = 2$), as can be seen from Fig. 3d, the states with wave vectors k from the center of the Brillouin zone still mainly pertain to the f states with $\sigma =\uparrow$, but they correspond not to the bottom energy values $E_{ks}^{(2)}$ any longer (as was the

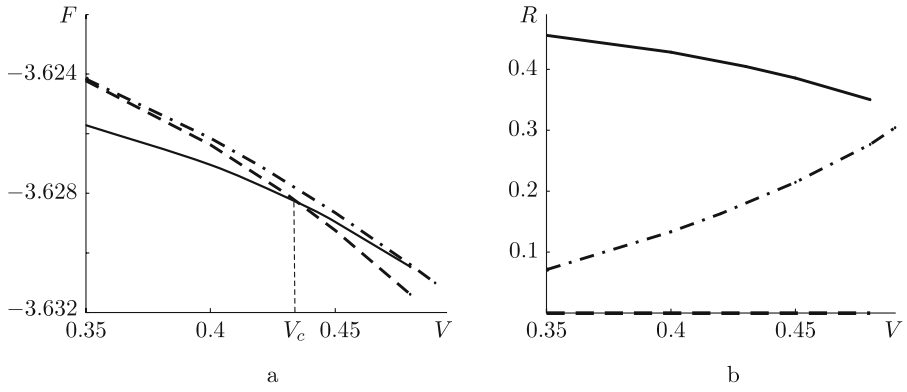

Fig. 4. Dependence of (a) the free energy F and (b) the AFM order parameter R on the hybridization V for three solutions: one paramagnetic (dashed line) and two magnetic (solid and dash-dotted lines).

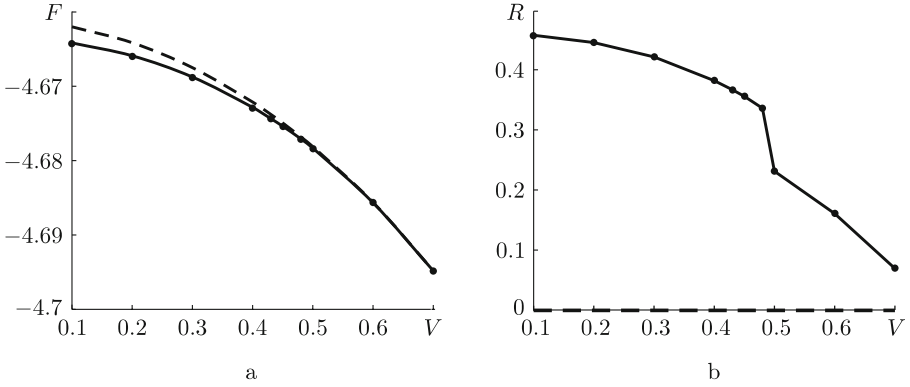

Fig. 5. Dependence of (a) the free energy F and (b) the AFM order parameter R on the hybridization V for the paramagnetic solution (dashed line) and the AFM solution (solid line).

case in Fig. 3a) but to the top ones. For localized electrons with $\sigma =\downarrow$, the maximum density of states occurs in this case at the bottom of the narrow band. It is obvious that as a result of the above inversion of $E_{ks}^{(2)}$, part of the localized spin-$\sigma=\uparrow$ electrons flow into states with $\sigma =\downarrow$, and the value of R decreases. As the temperature approaches $T_{\rm N}$, the bottom gap (between the $j = 1$ and $j = 2$ bands) decreases and then vanishes (Fig. 3e), while the top one (the hybridization gap of the paraphase) persists. The transition into the paramagnetic phase at $T = T_{\rm N}$ is followed by a leveling off of the densities of f-electron states with different spin moment projections (there is only a solid line in Fig. 3f), which is precisely the reason that R vanishes.

As the hybridization parameter, the temperature, or the magnetic field varies, the ground state of the system changes. The self-consistency equations can then admit several competing solutions in some domains of the phase diagram. A specific solution is selected as the stable phase based on the minimality of the free energy value. This thermodynamic potential can be computed based on representation (22) for the Hamiltonian $\widehat{\mathscr{H}}$. In this case, the free energy is given by

$$F(T,V,N) = -T\sum_{j=1}^{4}\sum_{ks}\log\left(1+\exp\left\{-\frac{E_{ks}^{(j)}-\mu}{T}\right\}\right) - \\ - 2NRmh_z + R^2N(I_0 - K_0\cos 2\theta) + 2\lambda N(e_0^2-1) + \mu N, \qquad (36)$$

where the eight branches $E_{ks}^{(j)}$ of the spectrum are found by solving dispersion equation (29).

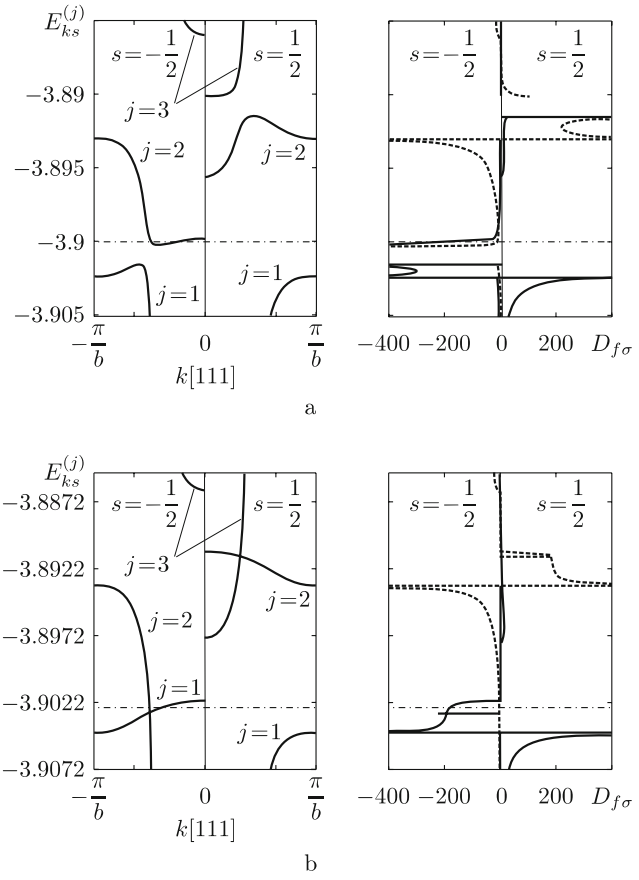

Fig. 6. The AFM HF quasiparticle spectrum and the density of f states in the canted phase in the neighborhood of the localized level with $H_c = 7.8 \cdot 10^{-3}$: (a) $H/H_c = 0.92$, (b) $H/H_c = 1$. The dash-dotted line shows the position of the chemical potential.

Depending on the value of the hybridization parameter, either the magnetic or the paramagnetic solution can have the lower energy. This is shown in Fig. 4. The computations were performed with the parameter values $E_0 = -2$, $K_0 = 0.02$, $J_0 = 0.5$, $n = 2.8$, $T = 1\,\mathrm{K}$, and $H = 0$. It can be seen from Fig. 4a that for the hybridization less than $V_c \approx 0.43$, the lowest free-energy value is realized in the AFM solution with the largest R (see Fig. 4b). But for $V > V_c$, the paramagnetic solution with $R = 0$ becomes energetically advantageous. The described change of the ground-state type demonstrates the destruction of the long-range AFM order in the localized subsystem with an increasing rate of the mixing process of collectivized states.

In the case where the ground-state type does not change as V increases, we nevertheless observe an essential suppression of the magnetic moment value of the rare-earth ion. This is demonstrated in Fig. 5, in computing which we changed two parameters compared with the computation presented in Fig. 4: we set $E_0 = -4$ and $n = 2.2$ and kept the other parameters the same. It can be seen that for all values of V, the energy of the solution describing the long-range magnetic order is lower than the energy of the paramagnetic solution. But the value of the magnetic moment R decreases from $R = 0.45$ (at $V = 0.1$) to $R = 0.06$ (at $V = 0.7$); it thus reaches the value that is experimentally observed in many AFM HF systems.

The effect of the magnetic field on spectral properties of AFM HF systems is represented in Fig. 6, where we show the quasimomentum dependences of the Fermi excitation energy $E_{ks}^{(j)}$ and the density $D_{f\sigma}$ of electron states in the neighborhood of the localized level. The model parameter values are chosen the

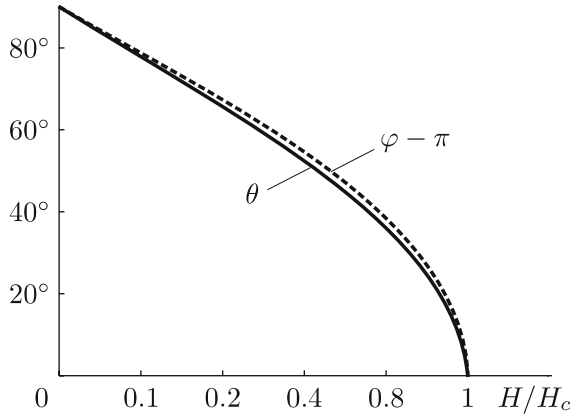

Fig. 7. The dependence of the angular canting θ and φ of magnetic sublattices on the external magnetic field.

same as in the computation of the graphs in Fig. 3, and the temperature is $T = 1\,\mathrm{K}$. The left panel in Fig. 6a shows the quasiparticle spectrum in the canted AFM phase computed at a magnetic field H less than the spin-flip transition field H_c. Comparing the dispersion curves in Figs. 6a and 3a shows that the strongest change in the spectrum occurs in the neighborhood of the f level and is accompanied by lifting the degeneracy with respect to the quantum number s. At $s = -1/2$, domains tending toward each other can be identified in the first (j=1) and the second (j=2) branches of the spectrum. A similar behavior is observed for the second and third branches with $s = +1/2$. The above domains of the spectrum continue approaching each other as the field strength increases and touch each other at $H = H_c$. The corresponding form of the spectrum is shown in the left panel in Fig. 6b.

The right panels in Figs. 6a and 6b show the graphs of the density of f-electron states in the same energy scale as for the corresponding dispersion curves. As previously, the solid and dashed lines denote the respective densities $D_{f\sigma}$ of f states for electrons with $\sigma = +1/2$ and with $\sigma = -1/2$. Because the densities of f states for bands with different s are different in a magnetic field, it is convenient to plot the function $D_{f\sigma}$ in different half-planes for different s, similarly to the spectral curves. It follows from the data in Fig. 6 that for $s = -1/2$, after the collapse of the magnetic moments of the sublattices at $H = H_c$, the top of the band $E^{(1)}_{k,-1/2}$ and the bottom of the band $E^{(2)}_{k,-1/2}$, mainly corresponding to f states with $\sigma =\uparrow$, can be interpreted as a single narrow band describing only spin-$\sigma =\uparrow$ electrons and continuing the band $E^{(1)}_{k,+1/2}$ (which also describes f electrons with $\sigma =\uparrow$) in Brillouin's scheme of reduced bands. A similar observation also applies to the second and the third branches of the spectrum with $s = +1/2$. The transition to the collinear ferromagnetic phase is thus accompanied by the disappearance of a narrow split band, and the resulting dispersion law can be represented as a standard mixon spectrum split with respect to σ by the magnetic and exchange fields.

We emphasize that in considering the spectrum of elementary excitations of the canted phase of metallic AFM HF systems, it has proved essential to account for the effect of collectivized electrons on the characteristics of the long-range magnetic order in the f subsystem. Their effect, underlain by the s–f-exchange and hybridization mechanisms, is negligibly small only for AFM systems with a low concentration of current carriers. But many rare-earth intermetallides are metals, and the effect of conductance electrons on the localized subsystem cannot be neglected when considering them. This explains the appearance in the theory of the canting angle φ of the collectivized subsystem. Furthermore, the relation between the canting angles would be trivial without taking the effect of c electrons into account ($\varphi = \theta + \pi$, for a positive s–f-exchange constant), but with the effect of conductance electrons on the f subsystem taken into

account, calculating the angle φ requires solving an additional self-consistency equation. In Fig. 7, we show the magnetic field dependence of the angular canting, constructed in a self-consistent computation of the graphs shown in Fig. 6. It can be seen that an increase in the field H leads to the canting of sublattices (the angles θ and φ decrease), and magnetic moments of the sublattices become collinear at the spin-flip transition point $H = H_c$ (the angles θ and φ then respectively become equal to 0 and π). It can be seen that the equality $\varphi = \theta + \pi$ is satisfied only in two limit cases: $H = 0$ and $H = H_c$. For intermediate values of the magnetic field, the difference between φ and $\theta + \pi$ reaches 3°. In the case under consideration, the vectors of means of the spin moments of localized and collectivized electrons for the same sublattice are oriented practically antiparallel to each other. The smallness of the obtained value of the difference between the angles is explained by the difference between the tangents of φ and θ being determined by the small quantity $\mu_B H/RJ_0$ in Eq. (17) at $L_0 = 0$ (just this case was chosen for simplicity in the calculations). For $L_0 \neq 0$, the difference between φ and θ increases. We note that despite the relatively small value of the angular difference noted above, it must nevertheless be taken into account because otherwise, as already noted, the heat capacity of the system in the canted phase can take negative values in the low-temperature domain.

8. Conclusions

The presented results were obtained with an approach based on an effective PAM Hamiltonian [22] that includes the exchange interaction both inside the localized subsystem and between the localized and collectivized subsystems. The main difference from the results in [11]–[14] amounts to at least two points.

First, the theory developed here is acceptable for describing AFM HF intermetallides with a metallic-type ground state because the restriction on the position of the chemical potential has been removed.

The second extension of the applicability domain of the proposed approach is associated with including magnetic fields such that the canting of the magnetic sublattices cannot be neglected. Taking this canting into account is the physical essence of our analysis of the HF spectrum features of AFM intermetallides in a magnetic field.

We note that in systematically accounting for the canting of the AFM structure in the subsystem of localized electrons, which occurs when an external magnetic field is imposed, the effect of the back-reaction of the magnetic degrees of freedom of collectivized electrons on the spin structure of the localized magnetic subsystem also turned out to be significant. This is especially important for metallic HF compounds, which have a high concentration of current carriers. This requires introducing different canting angles (θ and φ) for the localized and collectivized electron subsystems and leads to an increase in the number of self-consistency equations.

We also note that from the mathematical standpoint, the key role in obtaining reasonable analytic expressions for self-consistent means was played by the unitary transformation introduced in (26), which allows partially diagonalizing an eight-dimensional matrix and representing it in terms of two fourth-order matrices. This considerably simplifies the procedure for deriving a closed system of seven integral self-consistency equations and allows writing it in a form convenient for numerical calculations.

The investigated properties of the spectrum and density of states of heavy quasiparticles in the AFM phase must be manifested in various galvanomagnetic properties of AFM HF intermetallides. Such experiments, including those on heat capacity measurements in a magnetic field, have been performed with many AFM HF systems: $PuGa_3$ [2], Ce_2Au_2Cd [3], $YbNiSi_3$ [4], and $PuPd_5Al_2$ [5]. The finding is that the magnetic field has a noticeable effect on the low-temperature heat capacity in the neighborhood of the Néel temperature. Theoretically describing the magnetic field effect on the heat capacity of such systems requires using the HF spectrum in the canted phase. But the corresponding numerical computations are beyond the scope of this paper.

Appendix

We give the expressions used to calculate the thermodynamic properties of AFM HF systems in the canted phase:

$$\langle\langle c_{k\sigma}|c^{+}_{k\sigma}\rangle\rangle_{\omega}=\frac{1}{2}\frac{A^{(cc)}_{\sigma\sigma}(k,\omega)}{D^{(4)}_{k\bar{\sigma}}(\omega)}+\frac{1}{2}\frac{B^{(cc)}_{\sigma\sigma}(k,\omega)}{D^{(4)}_{k\sigma}(\omega)}, \tag{37}$$

where

$$\begin{aligned}
A^{(cc)}_{\sigma\sigma}(k,\omega)&=[(\omega-E_0-\lambda)^2-\sigma^2\bar{H}^2](\omega-t_k-\Gamma_k\cos\varphi-\sigma\widetilde{H})-\\
&-(\omega-E_0-\lambda)(u_k^2\cos\varphi+v_k^2)-\\
&-\sigma\bar{H}[u_k^2\cos\theta+\cos(\varphi+\theta)|\widetilde{W}_k|^2+\cos(\varphi-\theta)|\widetilde{V}_k|^2],\\
B^{(cc)}_{\sigma\sigma}(k,\omega)&=[(\omega-E_0-\lambda)^2-\sigma^2\bar{H}^2](\omega-t_k+\Gamma_k\cos\varphi-\sigma\widetilde{H})+\\
&+(\omega-E_0-\lambda)(u_k^2\cos\varphi-v_k^2)+\\
&+\sigma\bar{H}[u_k^2\cos\theta-\cos(\varphi+\theta)|\widetilde{W}_k|^2-\cos(\varphi-\theta)|\widetilde{V}_k|^2];
\end{aligned} \tag{38}$$

$$\langle\langle c_{k\bar{\sigma}}|c^{+}_{k\sigma}\rangle\rangle_{\omega}=\frac{1}{2}\frac{A^{(cc)}_{\bar{\sigma}\sigma}(k,\omega)}{D^{(4)}_{k\bar{\sigma}}(\omega)}+\frac{1}{2}\frac{B^{(cc)}_{\bar{\sigma}\sigma}(k,\omega)}{D^{(4)}_{k\sigma}(\omega)}, \tag{39}$$

where

$$\begin{aligned}
A^{(cc)}_{\bar{\sigma}\sigma}(k,\omega)&=2\sigma\sin\varphi\{\Gamma_k[(\omega-E_0-\lambda)^2-\sigma^2\bar{H}^2]+u_k^2(\omega-E_0-\lambda)\}+\\
&+2\sigma^2\bar{H}[(\widetilde{W}_k^{*}\widetilde{V}_k-\widetilde{V}_k^{*}\widetilde{W}_k)\sin\theta+\sin(\varphi+\theta)|\widetilde{W}_k|^2+\sin(\varphi-\theta)|\widetilde{V}_k|^2],\\
B^{(cc)}_{\bar{\sigma}\sigma}(k,\omega)&=-2\sigma\sin\varphi\{(\Gamma_k[(\omega-E_0-\lambda)^2-\sigma^2\bar{H}^2]+u_k^2(\omega-E_0-\lambda)\}+\\
&+2\sigma^2\bar{H}[(\widetilde{V}_k^{*}\widetilde{W}_k-\widetilde{W}_k^{*}\widetilde{V}_k)\sin\theta+\sin(\varphi+\theta)|\widetilde{W}_k|^2+\sin(\varphi-\theta)|\widetilde{V}_k|^2];
\end{aligned} \tag{40}$$

$$\langle\langle a_{k\sigma}|c^{+}_{k\sigma}\rangle\rangle_{\omega}=\frac{1}{2}\frac{A^{(ac)}_{\sigma\sigma}(k,\omega)}{D^{(4)}_{k\bar{\sigma}}(\omega)}+\frac{1}{2}\frac{B^{(ac)}_{\sigma\sigma}(k,\omega)}{D^{(4)}_{k\sigma}(\omega)}, \tag{41}$$

where

$$\begin{aligned}
A^{(ac)}_{\sigma\sigma}(k,\omega)&=-[(\omega-E_0-\lambda)^2-\sigma^2\bar{H}^2](\omega-t_k-\Gamma_k\cos\varphi-\sigma\widetilde{H})+\\
&+(\omega-E_0-\lambda)(u_k^2\cos\varphi+v_k^2)+\\
&[]+\sigma\bar{H}[u_k^2\cos\theta+\cos(\varphi+\theta)|\widetilde{W}_k|^2+\cos(\varphi-\theta)|V_k|^2],\\
B^{(ac)}_{\sigma\sigma}(k,\omega)&=[(\omega-E_0-\lambda)^2-\sigma^2\bar{H}^2](\omega-t_k+\Gamma_k\cos\varphi-\sigma\widetilde{H})+\\
&+(\omega-E_0-\lambda)(u_k^2\cos\varphi-v_k^2)+\\
&+\sigma\bar{H}[u_k^2\cos\theta-\cos(\varphi+\theta)|\widetilde{W}_k|^2-\cos(\varphi-\theta)|V_k|^2];
\end{aligned} \tag{42}$$

$$\langle\langle a_{k\bar{\sigma}}|c^{+}_{k\sigma}\rangle\rangle_{\omega}=\frac{1}{2}\frac{A^{(ac)}_{\bar{\sigma}\sigma}(k,\omega)}{D^{(4)}_{k\bar{\sigma}}(\omega)}+\frac{1}{2}\frac{B^{(ac)}_{\bar{\sigma}\sigma}(k,\omega)}{D^{(4)}_{k\sigma}(\omega)}, \tag{43}$$

where

$$A^{(ac)}_{\bar\sigma\sigma}(k,\omega) = 2\sigma\sin\varphi\{\Gamma_k[(\omega - E_0 - \lambda)^2 - \sigma^2\bar H^2] + u_k^2(\omega - E_0 - \lambda)\} +$$

$$+ \frac{\bar H}{2}[(\widetilde{W}_k^*\widetilde{V}_k - \widetilde{V}_k^*\widetilde{W}_k)\sin\theta + \sin(\varphi+\theta)|\widetilde{W}_k|^2 + \sin(\varphi-\theta)|\widetilde{V}_k|^2],$$

$$B^{(ac)}_{\bar\sigma\sigma}(k,\omega) = 2\sigma\sin\varphi\{\Gamma_k[(\omega - E_0 - \lambda)^2 - \sigma^2\bar H^2] + u_k^2(\omega - E_0 - \lambda)\} +$$

$$+ \frac{\bar H}{2}[(\widetilde{W}_k^*\widetilde{V}_k - \widetilde{V}_k^*\widetilde{W}_k)\sin\theta - \sin(\varphi+\theta)|\widetilde{W}_k|^2 - \sin(\varphi-\theta)|\widetilde{V}_k|^2]; \tag{44}$$

$$\langle\langle d_{k\sigma}|c^+_{k\sigma}\rangle\rangle_\omega = \frac{1}{2}\frac{A^{(dc)}_{\sigma\sigma}(k,\omega)}{D^{(4)}_{k\bar\sigma}(\omega)} + \frac{1}{2}\frac{B^{(dc)}_{\sigma\sigma}(k,\omega)}{D^{(4)}_{k\sigma}(\omega)}, \tag{45}$$

where

$$A^{(dc)}_{\sigma\sigma}(k,\omega) = (\omega - E_0 - \lambda - \sigma\bar H)\{(\omega - t_k - \sigma\widetilde H)[{V_k^{(c)}}^*(\varphi-\theta) - {W_k^{(c)}}^*(\varphi+\theta)] +$$

$$+ \Gamma_k[{W_k^{(c)}}^*(\varphi-\theta) - {V_k^{(c)}}^*(\varphi+\theta)]\} +$$

$$+ (\widetilde{W}_k^{*2} - \widetilde{V}_k^{*2})[V_k^{(c)}(\varphi-\theta) + W_k^{(c)}(\varphi+\theta)],$$

$$B^{(dc)}_{\sigma\sigma}(k,\omega) = (\omega - E_0 - \lambda - \sigma\bar H)\{(\omega - t_k - \sigma\widetilde H)[{V_k^{(c)}}^*(\varphi-\theta) + {W_k^{(c)}}^*(\varphi+\theta)] +$$

$$+ \Gamma_k[{W_k^{(c)}}^*(\varphi-\theta) + {V_k^{(c)}}^*(\varphi+\theta)]\} +$$

$$+ (\widetilde{W}_k^{*2} - \widetilde{V}_k^{*2})[V_k^{(c)}(\varphi-\theta) - W_k^{(c)}(\varphi+\theta)]; \tag{46}$$

$$\langle\langle d_{k\bar\sigma}|c^+_{k\sigma}\rangle\rangle_\omega = \frac{1}{2}\frac{A^{(dc)}_{\bar\sigma\sigma}(k,\omega)}{D^{(4)}_{k\bar\sigma}(\omega)} + \frac{1}{2}\frac{B^{(dc)}_{\bar\sigma\sigma}(k,\omega)}{D^{(4)}_{k\sigma}(\omega)}, \tag{47}$$

where

$$A^{(dc)}_{\bar\sigma\sigma}(k,\omega) = (\omega - E_0 - \lambda + \sigma\bar H)\{(\omega - t_k - \sigma\widetilde H)[{V_k^{(s)}}^*(\varphi-\theta) + {W_k^{(s)}}^*(\varphi+\theta)] +$$

$$+ \Gamma_k[{W_k^{(s)}}^*(\varphi-\theta) + {V_k^{(s)}}^*(\varphi+\theta)]\} +$$

$$+ (\widetilde{W}_k^{*2} - \widetilde{V}_k^{*2})[V_k^{(s)}(\varphi-\theta) - W_k^{(s)}(\varphi+\theta)],$$

$$B^{(dc)}_{\bar\sigma\sigma}(k,\omega) = (\omega - E_0 - \lambda + \sigma\bar H)\{(\omega - t_k - \sigma\widetilde H)[{V_k^{(s)}}^*(\varphi-\theta) - {W_k^{(s)}}^*(\varphi+\theta)] +$$

$$+ \Gamma_k[{W_k^{(s)}}^*(\varphi-\theta) - {V_k^{(s)}}^*(\varphi+\theta)]\} +$$

$$+ (\widetilde{W}_k^{*2} - \widetilde{V}_k^{*2})[V_k^{(s)}(\varphi-\theta) + W_k^{(s)}(\varphi+\theta)]; \tag{48}$$

$$\langle\langle b_{k\sigma}|c^+_{k\sigma}\rangle\rangle_\omega = \frac{1}{2}\frac{A^{(bc)}_{\sigma\sigma}(k,\omega)}{D^{(4)}_{k\bar\sigma}(\omega)} + \frac{1}{2}\frac{B^{(bc)}_{\sigma\sigma}(k,\omega)}{D^{(4)}_{k\sigma}(\omega)}, \tag{49}$$

where

$$A^{(bc)}_{\sigma\sigma}(k,\omega) = (\omega - E_0 - \lambda - \sigma\bar{H})\{(\omega - t_k - \sigma\widetilde{H})[W^{(c)^*}_k(\varphi+\theta) - V^{(c)^*}_k(\varphi-\theta)] +$$

$$+ \Gamma_k[V^{(c)^*}_k(\varphi+\theta) - W^{(c)^*}_k(\varphi-\theta)]\} +$$

$$+ (\widetilde{V}^{*2}_k - \widetilde{W}^{*2}_k)[V^{(c)}_k(\varphi-\theta) + W^{(c)}_k(\varphi+\theta)],$$

$$B^{(bc)}_{\sigma\sigma}(k,\omega) = (\omega - E_0 - \lambda - \sigma\bar{H})\{(\omega - t_k - \sigma\widetilde{H})[W^{(c)^*}_k(\varphi+\theta) + V^{(c)^*}_k(\varphi-\theta)] +$$

$$+ \Gamma_k[V^{(c)^*}_k(\varphi+\theta) + W^{(c)^*}_k(\varphi-\theta)]\} +$$

$$+ (\widetilde{V}^{*2}_k - \widetilde{W}^{*2}_k)[W^{(c)}_k(\varphi+\theta) - V^{(c)}_k(\varphi-\theta)]; \tag{50}$$

$$\langle\langle b_{k\bar{\sigma}} | c^+_{k\sigma}\rangle\rangle_\omega = \frac{1}{2}\frac{A^{(bc)}_{\bar{\sigma}\sigma}(k,\omega)}{D^{(4)}_{k\bar{\sigma}}(\omega)} + \frac{1}{2}\frac{B^{(bc)}_{\bar{\sigma}\sigma}(k,\omega)}{D^{(4)}_{k\sigma}(\omega)}, \tag{51}$$

where

$$A^{(bc)}_{\bar{\sigma}\sigma}(k,\omega) = (\omega - E_0 - \lambda + \sigma\bar{H})\{(\omega - t_k - \sigma\widetilde{H})[V^{(s)^*}_k(\varphi-\theta) + W^{(s)^*}_k(\varphi+\theta)] +$$

$$+ \Gamma_k[W^{(s)^*}_k(\varphi-\theta) + V^{(s)^*}_k(\varphi+\theta)]\} +$$

$$+ (\widetilde{W}^{*2}_k - \widetilde{V}^{*2}_k)[V^{(s)}_k(\varphi-\theta) - W^{(s)}_k(\varphi+\theta)],$$

$$B^{(bc)}_{\bar{\sigma}\sigma}(k,\omega) = (\omega - E_0 - \lambda + \sigma\bar{H})\{(\omega - t_k - \sigma\widetilde{H})[-V^{(s)^*}_k(\varphi-\theta) + W^{(s)^*}_k(\varphi+\theta)] +$$

$$+ \Gamma_k[-W^{(s)^*}_k(\varphi-\theta) + V^{(s)^*}_k(\varphi+\theta)]\} +$$

$$+ (\widetilde{W}^{*2}_k - \widetilde{V}^{*2}_k)[-V^{(s)}_k(\varphi-\theta) - W^{(s)}_k(\varphi+\theta)]; \tag{52}$$

and

$$\langle\langle d_{k\sigma} | d^+_{k\sigma}\rangle\rangle_\omega = \frac{1}{2}\frac{A^{(dd)}_{\sigma\sigma}(k,\omega)}{D^{(4)}_{k\bar{\sigma}}(\omega)} + \frac{1}{2}\frac{B^{(dd)}_{\sigma\sigma}(k,\omega)}{D^{(4)}_{k\sigma}(\omega)}, \tag{53}$$

where

$$A^{(dd)}_{\sigma\sigma}(k,\omega) = (\omega - E_0 - \lambda - \sigma\bar{H})[(\omega - t_k)^2 - \Gamma^2_k - \sigma^2\widetilde{H}^2 - 2\sigma\widetilde{H}\Gamma_k\cos\varphi] -$$

$$- (\omega - t_k)(v^2_k + u^2_k\cos\theta) - \Gamma_k(u^2_k + v^2_k\cos\theta) -$$

$$- \sigma\widetilde{H}\big[|\widetilde{W}_k|^2\cos(\varphi+\theta) + |\widetilde{V}_k|^2\cos(\varphi-\theta) + u^2_k\cos\varphi\big],$$

$$B^{(dd)}_{\sigma\sigma}(k,\omega) = (\omega - E_0 - \lambda - \sigma\bar{H})[(\omega - t_k)^2 - \Gamma^2_k - \sigma^2\widetilde{H}^2 + 2\sigma\widetilde{H}\Gamma_k\cos\varphi] -$$

$$- (\omega - t_k)(v^2_k - u^2_k\cos\theta) - \Gamma_k(u^2_k - v^2_k\cos\theta) -$$

$$- \sigma\widetilde{H}\big[|\widetilde{W}_k|^2\cos(\varphi+\theta) + |\widetilde{V}_k|^2\cos(\varphi-\theta) - u^2_k\cos\varphi\big]. \tag{54}$$

Acknowledgments. This paper was supported by the Russian Foundation for Basic Research (Grant No. 07-02-00226), the Siberian Branch, Russian Academy of Sciences (Integrated Project No. 53), and the program "Strong Electron Correlations" of the Physics Division, Russian Academy of Sciences.

REFERENCES

1. C. M. Varma, W. Weber, and L. J. Randall, *Phys. Rev. B*, **33**, 1015–1019 (1986).
2. P. Boulet, E. Colineau, F. Wastin, P. Javorsky, J. C. Griveau, J. Rebizant, G. R. Stewart, and E. D. Bauer, *Phys. Rev. B*, **72**, 064438 (2005).
3. S. Rayaprol and R. Pottgen, *Phys. Rev. B*, **72**, 214435 (2005).
4. S. L. Bud'ko, P. C. Canfield, M. A. Avila, and T. Takabatake, *Phys. Rev. B*, **75**, 094433 (2007).
5. K. Gofryk, J.-C. Griveau, E. Colineau, and J. Rebizant, *Phys. Rev. B*, **77**, 092405 (2008).
6. N. E. Sluchanko, A. V. Bogach, V. V. Glushkov, S. V. Demishev, N. A. Samarin, G. S. Burkhanov, and O. D. Chistyakov, *JETP Lett.*, **76**, 26–29 (2002).
7. P. A. Alekseev, J.-M. Mignot, K. S. Nemkovski, V. N. Lazukov, E. V. Nefeodova, A. P. Menushenkov, A. V. Kuznetsov, R. I. Bewley, and A. V. Gribanov, *JETP*, **105**, 14–17 (2007).
8. M. I. Ignatov, A. V. Bogach, G. S. Burkhanov, V. V. Glushkov, S. V. Demishev, A. V. Kuznetsov, O. D. Chistyakov, N. Yu. Shitsevalova, and N. E. Sluchanko, *JETP*, **105**, 58–61 (2007).
9. A. V. Bogach, G. S. Burkhanov, V. V. Glushkov, S. V. Demishev, O. D. Chistyakov, and N. E. Sluchanko, *JETP*, **105**, 108–111 (2007).
10. P. Coleman, *Phys. Rev. B*, **29**, 3035–3044 (1984).
11. V. Dorin and P. Schlottmann, *Phys. Rev. B*, **46**, 10800–10807 (1992).
12. B. Möller and P. Wölfle, *Phys. Rev. B*, **48**, 10320–10326 (1993).
13. E. Halvorsen and G. Czycholl, *J. Phys.*: *Condens. Matter*, **8**, 1775–1783 (1996).
14. S.-J. Sun, M.-F. Yang, and T.-M. Hong, *Phys. Rev. B*, **48**, 16127–16130 (1993).
15. J. R. Schrieffer and P. A. Wolff, *Phys. Rev.*, **149**, 491–492 (1966).
16. C. Lacroix and M. Cyrot, *Phys. Rev. B*, **20**, 1969–1976 (1979).
17. C. Proetto and A. López, *Phys. Rev. B*, **24**, 3031–3036 (1981).
18. V. A. Moskalenko and N. B. Perkins, *Theor. Math. Phys.*, **121**, 1654–1665 (1999).
19. D. F. Digor, P. Entel, M. Marinaro, V. A. Moskalenko, and N. B. Perkins, *Theor. Math. Phys.*, **127**, 664–675 (2001).
20. A. Hübsch and K. W. Becker, *Eur. Phys. J. B*, **52**, 345–353 (2006).
21. Z. Liang-Jian and Z. Qing-Qi, *J. Magn. Magn. Mater.*, **109**, 237–242 (1992).
22. V. V. Val'kov and D. M. Dzebisashvili, *Theor. Math. Phys.*, **157** (1565-1576).
23. S. V. Tyablikov, *Methods in the Quantum Theory of Magnetism* [in Russian], Nauka, Moscow (1965); English transl., Plenum, New York (1967).